atmosphere

Article

Longitudinal Variation of Thermospheric Density during Low Solar Activity from APOD Observations

Guangming Chen [1,*], Xie Li [1], Maosheng He [2], Shushi Liu [1], Haijun Man [1], Hong Gao [3] and Yongping Li [4]

1 Science and Technology on Aerospace Flight Dynamics Laboratory, Beijing Aerospace Control Center, Beijing 100094, China
2 Independent Researcher, Wiesengrund 2a, 18225 Kuehlungsborn, Germany
3 State Key Laboratory of Space Weather, National Space Science Center, Chinese Academy of Sciences, Beijing 100190, China
4 Beijing Key Laboratory of Space Environment Exploration, National Space Science Center, Chinese Academy of Sciences, Beijing 100190, China
* Correspondence: chen_g_m@126.com

Abstract: The longitudinal distribution of upper atmospheric density has been broadly studied. However, the studies mostly focused on 24 h averaged distribution. This study presents the longitudinal distribution of thermospheric density at dawn and dusk, using observations collected by the atmospheric density detector onboard the Chinese satellite APOD (Atmospheric Density Detection and Precise Orbit Determination) during low solar activity. The APOD observations show a significant relative longitudinal variation of thermospheric density with global maxima ($\Delta\rho_{rmax}$) near the geomagnetic pole, especially in the winter hemisphere. The annual maximum of $\Delta\rho_{rmax}$ appears in the Southern Hemisphere around the June solstices and reaches 26.3% and 39.6% at dawn and dusk, respectively. The auroral heating and meridional wind might play a significant role in the longitudinal variation of thermospheric density. We further compare the APOD observations with the semi-empirical atmospheric model MSIS (Mass Spectrometer Incoherent Scatter Radar) 2.0 predictions under low solar activity conditions. The MSIS 2.0 model reproduces similar longitudinal variations to the observations, with hemispheric asymmetry. The longitudinal variation of thermospheric density from APOD should be related to the distribution of the atmospheric average molecular weight from the model. More observational data are needed to verify the results of this study further.

Keywords: thermospheric density; longitudinal distribution; dawn; dusk; low solar activity; APOD

check for updates

Citation: Chen, G.; Li, X.; He, M.; Liu, S.; Man, H.; Gao, H.; Li, Y. Longitudinal Variation of Thermospheric Density during Low Solar Activity from APOD Observations. *Atmosphere* **2023**, *14*, 155. https://doi.org/10.3390/atmos14010155

Academic Editor: Annick Pouquet

Received: 27 November 2022
Revised: 26 December 2022
Accepted: 28 December 2022
Published: 10 January 2023

Copyright: © 2023 by the authors. Licensee MDPI, Basel, Switzerland. This article is an open access article distributed under the terms and conditions of the Creative Commons Attribution (CC BY) license (https://creativecommons.org/licenses/by/4.0/).

1. Introduction

Variations in upper thermospheric density can cause perturbations in spacecraft orbits [1–3]. Thus, the variations under different space weather conditions have attracted broad interest [4–8]. One of these variations is the longitude/UT variation of the thermospheric density. The magnetospheric energy deposition could induce thermospheric longitudinal variations through the auroral precipitation and Joule heating [4,9]. Observational studies were typically based on in-situ measurements collected by slowly-processing polar satellites in low earth orbits subject to an inherent sampling limitation associated with the orbits. The orbits typically take several months to cover 24 h local time. Therefore, the results often entangle the local time variation with the seasonal variation. To conquer this problem, Xu et al. [10] developed a method by averaging the data across multi-years. The method could produce 24 h averaged longitudinal variations in different seasons, but studying the longitudinal variations at different local times is still challenging. Using observations by a detector onboard a sun-synchronous satellite will avoid this problem and produce longitudinal distribution at a fixed local time.

The longitudinal variations of thermospheric density at ~200 km at 1030 LT and 2230 LT have been studied from the SETA (Satellite Electrostatic Triaxial Accelerometer) experiments in a sun-synchronous orbit [11,12]. The seasonal variations of thermospheric mass density at dawn and dusk have been examined from the GOCE (Gravity field and steady-state Ocean Circulation Explorer) satellite observations at 270 km [13]. However, the longitudinal variations of upper thermospheric density are rarely studied above 300 km at fixed local times. This is important because most low-orbit spacecraft fly through the upper thermosphere. Furthermore, the longitudinal variations at dawn and dusk are unknown. Given that the horizontal gradient of solar radiation is prominent in the sectors, a large gradient of thermospheric density is also expected; therefore, the longitudinal distribution may differ from that of other local times [14]. The Chinese APOD satellite flies in a circular sun-synchronous orbit carrying an Atmospheric Density Detector (ADD) and detects the thermospheric density around the terminator [15,16]. It allows us to study the longitudinal variations around the terminator in the upper thermosphere during low solar activity.

Calabia et al. [17] assessed a new thermospheric mass density model using the APOD observations. Zhang et al. [18] provided the seasonal oscillations of thermospheric density from the APOD and other observations. The current paper studies the longitudinal distributions of thermospheric density at 460 km at dawn and dusk using the measurements from the Chinese satellite APOD. The longitudinal distributions from APOD are compared with those from the NRLMSIS 2.0 model [19], which is the newest version of the semi-empirical model series of Mass Spectrometer Incoherent Scatter Radar (MSIS) [20]. This work focuses on answering the following three open questions: (1) What is the longitudinal variation of the thermospheric density at dawn dusk in different seasons under low solar activity conditions? (2) Does the longitudinal variation at dawn differ from that at dusk? (3) Is the longitudinal variation from the MSIS model similar to that from APOD?

2. Data and Methods

The Chinese APOD satellites, including APOD-A, -B, -C, and -D, were launched into circular sun-synchronous orbits in 2015. Onboard APOD-A is an Atmospheric Density Detector (ADD), which samples the thermospheric density at a rate of 1 Hz, corresponding to a spatial resolution of ~8 km. This paper uses the thermospheric density observations only from APOD-A and refers to APOD-A as APOD. The principle of the ADD and the data processing method were detailed by Li et al. [15] and Tang et al. [16]. The longitudinal distribution of thermospheric mass density is constructed using the observations under quiet geomagnetic conditions (ap < 10) in 2017 and 2018 when the sun was at a low activity level with an annual average of F10.7 around 77 and 70, respectively.

The data observed are processed in the descending and ascending legs separately. These two legs cross the equator at the local time around 0730 LT and 1930 LT and hereinafter are referred to as dawn and dusk sectors. To exclude the altitude and local time variations associated with the APOD orbit, we normalized the mass densities using the MSIS 2.0 model [19] to fixed reference heights of 460 km [4,21] at local times 0730 LT and 1930 LT, respectively. In each sector and each month, the data are binned in grids of 5° in latitude and 20° in longitude from 82.5° S to 82.5° N. Figure 1, as an example, displays a histogram of the data collected in July. The histogram indicates that the observations are sufficient at all given grids, allowing reliable statistics.

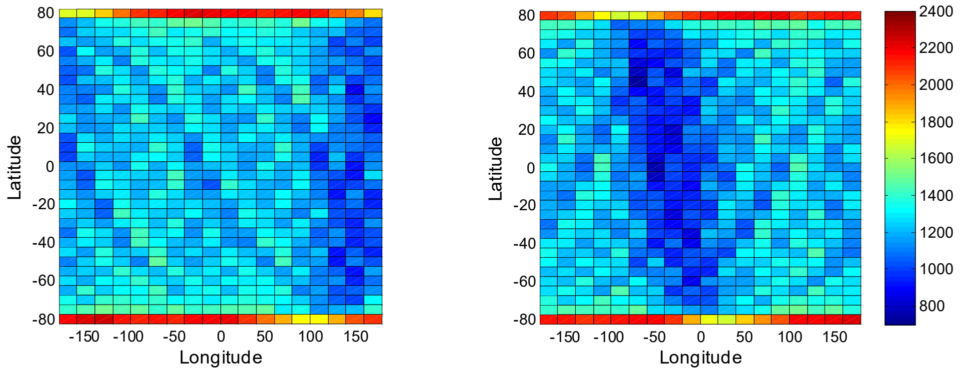

Figure 1. Global distributions of the samplings from APOD at dawn (**left**) and dusk (**right**) in July.

The monthly averaged APOD density (ρ) is calculated in each grid at dawn or dusk, respectively. Then Equation (1) is used to obtain the zonal mean of the monthly averaged thermospheric density ($\overline{\rho}$),

$$\overline{\rho} = \frac{1}{2\pi}\int_{0}^{2\pi} \rho \mathrm{d}\lambda \tag{1}$$

where λ denotes longitude.

Equation (2) is used to estimate the relative longitudinal variation of thermospheric density,

$$\Delta\rho_r = \rho/\overline{\rho} - 1 \tag{2}$$

The semi-empirical model series of Mass Spectrometer Incoherent Scatter Radar (MSIS) [20] are widely used in thermospheric research and aerospace engineering and can predict the composition, total mass density, number density, and temperature from the ground to the exosphere. The semi-empirical model series has been upgraded to the latest version as NRLMSIS 2.0 [19], in which the development focuses primarily on altitudes below 100 km; N_2 and O densities in the thermosphere were also improved. Predictions of spacecraft orbits are subject to the uncertainty of the atmospheric model [22]. Note that NRLMSIS 2.0 will be referred to simply as MSIS hereafter. Using the MSIS, we calculated thermospheric densities along the APOD orbit and reproduced the longitudinal distributions.

The empirical model HL-TWiM (High-latitude Thermospheric Wind Model) presents a good characterization of the high-latitude neutral winds in geomagnetic coordinates for both hemispheres at altitudes between 210 and 320 km [23]. The model synthesizes the most historical high-latitude wind measurements (45–90 Mlat) and provides a valuable specification of thermospheric neutral wind as a function of DOY (Day Of Year), latitude, longitude, local time, and geomagnetic conditions in magnetic coordinates. The paper uses this model to study the relationship between the thermospheric wind and the longitudinal distribution of the thermospheric density.

3. Results and Discussion

Figures 2 and 3 show the global distributions of relative longitudinal variation ($\Delta\rho_r$) from APOD in different months at dawn and dusk, respectively. The most prominent feature is one region with high $\Delta\rho_r$ in each hemisphere. In the northern hemisphere, the zonal maximum of $\Delta\rho_r$ ($\Delta\rho_{rmax}$) appears at 60–100° W at dawn except for 40° W in June and appears at 80–120° W at dusk except 60° W in November. In the southern hemisphere, $\Delta\rho_{rmax}$ appears at 80–120° E at dawn except 60° E in January and appears at 160–200° E at dusk except 140° E in February. From November to February, the high-density region in the northern hemisphere is more pronounced. The global $\Delta\rho_{rmax}$ appears at 65–75° N in latitude and 60–120° W in longitude. From April to September, the high-density region in the Southern Hemisphere is more pronounced, and $\Delta\rho_{rmax}$ is located at 50–75° S and 100–

180° E. The location of $\Delta\rho_{rmax}$ is close to the geomagnetic pole, which was at (~83° N, ~84° W) in the northern hemisphere and (~75° S, ~125° E) in the Southern Hemisphere in 2017–2018, according to the altitude-adjusted corrected geomagnetic (AACGM) coordinates [24]. It is known that auroral heating occurs mainly around the geomagnetic pole [25–28], which causes the enhancement of temperature (thermospheric density) in the lower (upper) thermosphere [29]. Thus, the maximum of $\Delta\rho_r$ occurring near the geomagnetic pole can be attributed to the aurora heating, including the aurora particles precipitation and Joule heating.

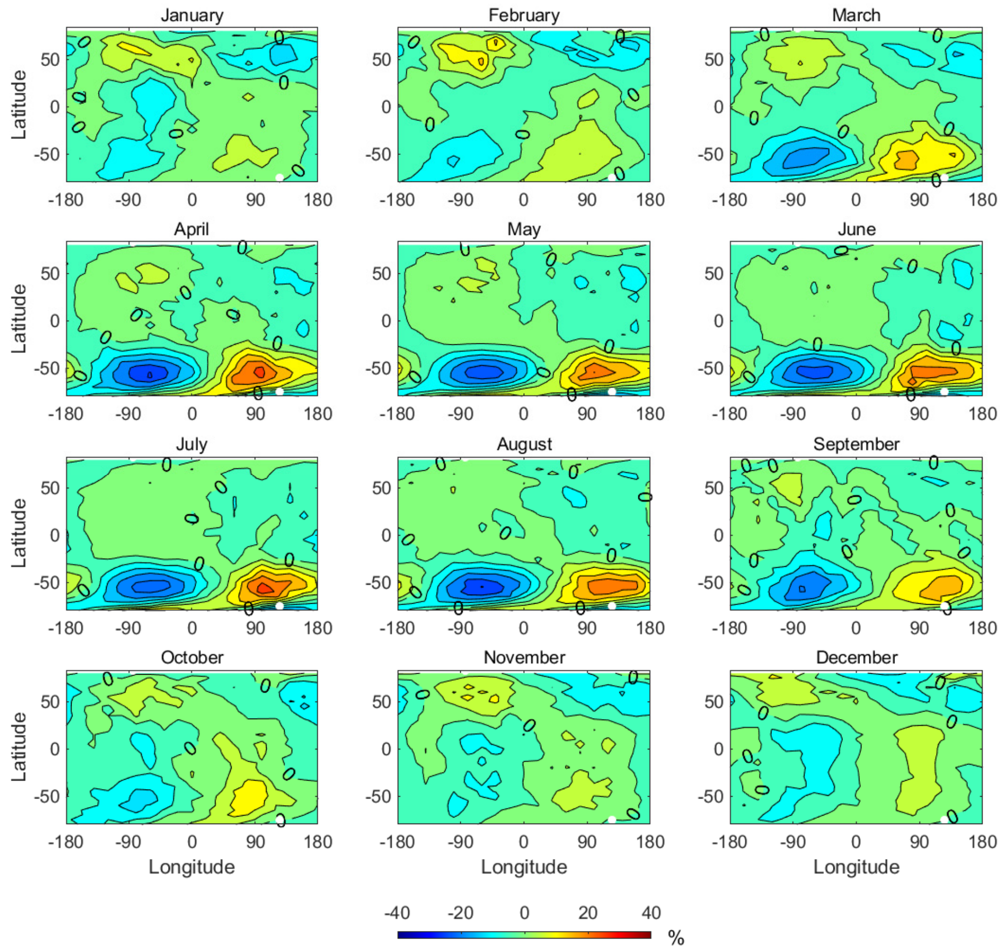

Figure 2. The global distributions of the relative longitudinal variation ($\Delta\rho_r$) from APOD at 0730 LT (dawn) in each month. White dots denote the position of the south geomagnetic pole.

Figures 2 and 3 show that the maximum of $\Delta\rho_r$ in the Southern Hemisphere is greater than in the Northern Hemisphere at both dawn and dusk from April to August. During November and February, the maximum of $\Delta\rho_r$ in the Northern Hemisphere is greater than in the Southern Hemisphere. For example, in December, the maximum of $\Delta\rho_r$ in the Northern Hemisphere is 13.2% and 25.4% at dawn and dusk, respectively, while the maximum in the Southern Hemisphere is only 9.0% and 7.1% at dawn and dusk, respectively. It indicates that $\Delta\rho_{rmax}$ in the winter hemisphere is higher than in the summer hemisphere around the solstices. The difference of $\Delta\rho_{rmax}$ between the summer and winter hemispheres may be caused by the difference in the solar EUV energy input into the thermosphere between the two hemispheres. At the same latitude in two hemispheres, the solar elevating angle in the winter hemisphere is smaller than in the summer, and some polar regions in the winter hemisphere are not even lit by the Sun. Therefore, the EUV energy input into the thermosphere and $\overline{\rho}$ in the winter hemisphere are much less than those in the summer hemisphere, which causes the lower background thermosphere density in the winter hemisphere. According to Equation (2), $\Delta\rho_r$ is inversely proportional to the value of $\overline{\rho}$. Thus, $\Delta\rho_{rmax}$ caused by the auroral heating in the winter hemisphere was more significant than in the summer hemisphere.

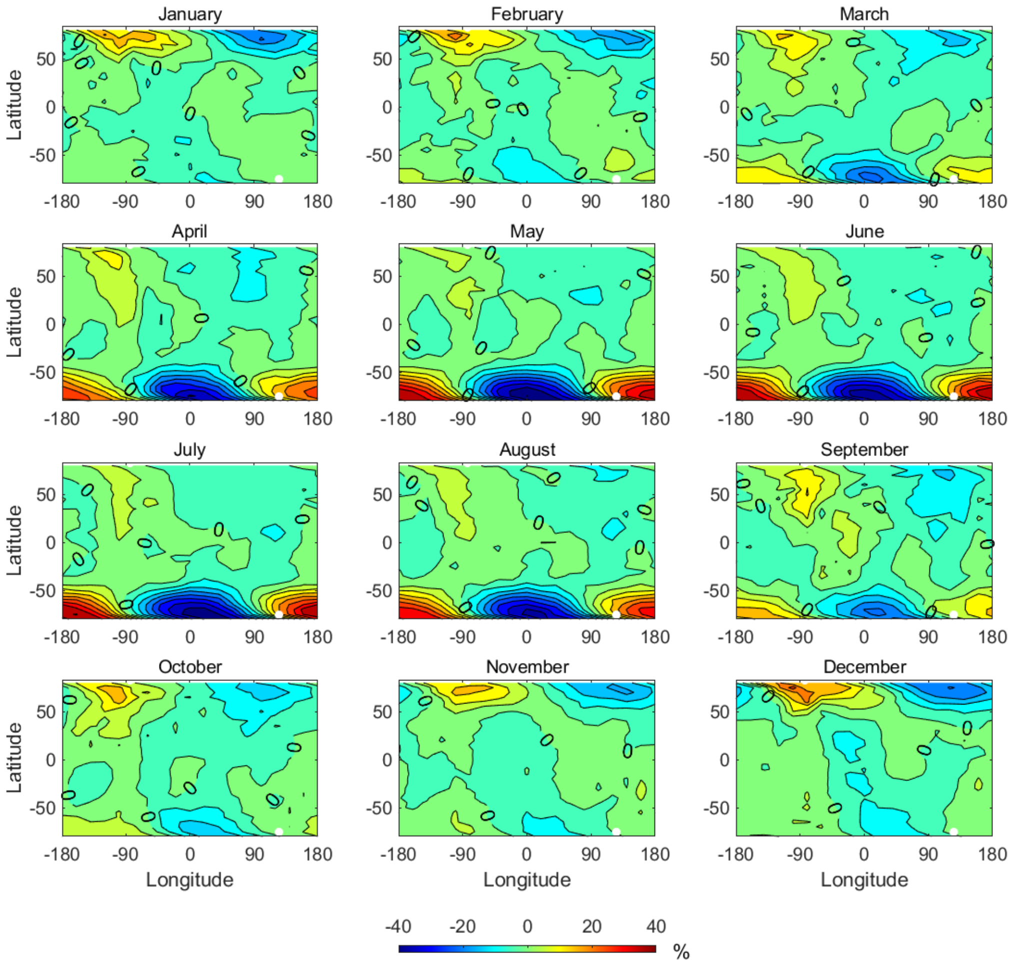

Figure 3. Same as Figure 2 except for the thermospheric densities at 1930 LT (dusk).

In Figures 2 and 3, the $\Delta\rho_{rmax}$ maximizes annually at 26.3% and 39.6% in July in the Southern Hemisphere near the geomagnetic pole (~75° S, ~125° E) at dawn and dusk, respectively. The annual maximum of $\Delta\rho_{rmax}$ in the Northern Hemisphere appears in February and December at dawn and dusk, with values of 15.8% and 25.4%, respectively. The annual maximum in the Southern Hemisphere is much greater than in the Northern Hemisphere. The difference in $\Delta\rho_{rmax}$ between the two hemispheres should be mainly caused by the different geomagnetic pole positions relative to the geographic poles. Since the aurora heating is mainly around the geomagnetic pole [25–28] and the southern geomagnetic pole is further off the geographical pole, the effects of auroral heating on the thermosphere in the Southern Hemisphere are harder to cover all longitudes. Thus, the longitudinal variation of thermospheric density in the Southern Hemisphere should be relatively stronger in the Northern Hemisphere under the same other conditions. Xu et al. [10] analyzed the longitudinal variation of thermospheric density using the CHAMP and GRACE satellite observations. Their results showed that the maximal longitude variations averaged for all local times also appear near the geomagnetic poles. Similar to the APOD observations, the CHAMP and GRACE satellite observations showed an apparent hemispheric asymmetry in the longitudinal structure, more pronounced in the Southern Hemisphere than in the Northern Hemisphere. To sum up, the main feature of the global distribution around the terminator from APOD is similar to the distribution averaged over all local times from GRACE.

There is a low-density region in each hemisphere, which is close to the high-density region in latitude and far away from the high-density region in longitude. In the Northern Hemisphere, the minimum of $\Delta\rho_r$ ($\Delta\rho_{rmin}$) appears at 80–160° E at dawn and appears at 80–140° W at dusk. In the Southern Hemisphere, $\Delta\rho_{rmin}$ appears at 60–100° W at dawn except for 40° W in November and appears at 0–40° E at dusk except for 60° E in December. $\Delta\rho_{rmin}$ in the Southern Hemisphere is less than in the Northern Hemisphere at both dawn and dusk from April to August. However, from November to February, the minima of $\Delta\rho_r$ in the Northern Hemisphere is less than in the Southern Hemisphere, which is in summer. For example, in the December Northern Hemisphere, the $\Delta\rho_r$ minimizes at −11.3% and −20.4% at dawn and dusk, respectively, while in the Southern Hemisphere it minimizes at −7.8% and −8.4% at dawn and dusk, respectively.

As is shown in Figures 2 and 3, the longitudinal variations of $\Delta\rho_r$ around the geomagnetic pole significantly expand to the middle and low latitudes. The expansion diminishes with latitude decreasing, and the values of $\Delta\rho_r$ at low latitudes vary between −10% and 10% in most months. The expansion also changes with the seasons. Near the solstices, the longitudinal variation around the geomagnetic pole in the summer hemisphere can control the low latitudes and extend to the other hemisphere. Otherwise, the longitudinal variations around the geomagnetic pole in the winter hemisphere have weaker impacts on the mid-low latitudes, although the maxima of $\Delta\rho_r$ in the winter hemisphere are larger. The difference in equatorward expansion could be related to the meridional wind in the mid-low latitudes. To clarify the contribution of meridional wind to the equatorward expansion and the asymmetry of $\Delta\rho_{rmax}$ between the two hemispheres, we calculated the meridional wind in the middle and high latitudes at dawn (0730 LT) and dusk (1930 LT) using the empirical model HL-TWiM. The seasonal distribution of meridional wind between 30–80° N at 84° W and 30–80° S at 125° E is given in the upper panel of Figure 4. According to Figure 4, during the solstices, the thermospheric prevailing meridional wind is equatorward in the summer hemisphere and at latitudes 30–40° N (S) in the winter hemisphere. The equatorward wind should facilitate the longitude variations of $\Delta\rho_{rmax}$ around the magnetic pole in the summer hemisphere extending to low latitudes. It may help reduce the value of $\Delta\rho_{rmax}$ in the summer hemisphere.

Figures 2 and 3 show that $\Delta\rho_{rmax}$ from APOD appears at (50–60° S, 80–140° E) at dawn and (70–75° S, ~180° E) at dusk from April to August. The global $\Delta\rho_{rmax}$ appears at (65–75° N, 60–120° W) at dawn and at (~75° N, 60–100° W) at dusk from November to February. Comparing the latitudes of $\Delta\rho_{rmax}$ at dawn and dusk, the latitudes of $\Delta\rho_{rmax}$ at dusk are higher and closer to the geomagnetic pole in the two hemispheres. According to the longitudes of $\Delta\rho_{rmax}$, the positions of $\Delta\rho_{rmax}$ at dusk are in the east of that at dawn, especially in the southern hemisphere. The difference between the latitudes where $\Delta\rho_{rmax}$ appears at dawn and dusk may be related to the meridional wind.

According to the HL-TWiM empirical model results in the upper panel in Figure 4, the mid-high latitude thermospheric wind is poleward with a maximum of 76 ms^{-1} at 50° S at dusk. At dawn, it is equatorward or poleward with lower values relative to dusk between 50° S and 75° S. Take December as an example. The thermospheric meridional wind between 50° N and 75° N is less than 15 ms^{-1} at dawn, weaker than that at dusk.

The largest meridional wind speed reaches above 50 ms^{-1}, around 60° N at dusk. The more intensive poleward wind might induce the location of $\Delta\rho_{rmax}$ extending to the polar region at dusk. In addition, the difference in longitudes where $\Delta\rho_{rmax}$ appears at dawn and dusk could be attributed to the zonal wind. From the lower panel of Figure 4, the zonal wind at the latitude where $\Delta\rho_{rmax}$ appears is westward in the two hemispheres at dawn. The westward wind facilitates the westward extension of $\Delta\rho_{rmax}$ at dawn. At dusk, the zonal wind at the latitude where $\Delta\rho_{rmax}$ appears is eastward in two hemispheres. The eastward wind facilitates the eastward extension in $\Delta\rho_{rmax}$ at dusk. The zonal winds could explain the difference in the longitude where $\Delta\rho_{rmax}$ appears at dawn and dusk. The zonal wind in the southern hemisphere reaches more than 70 ms^{-1}, which is more significant than in the Northern Hemisphere. Thus, the difference in the longitude, where $\Delta\rho_{rmax}$ appears between dawn and dusk, is pronounced in the Southern Hemisphere. The exact reason may need further study through additional observation and numerical simulation.

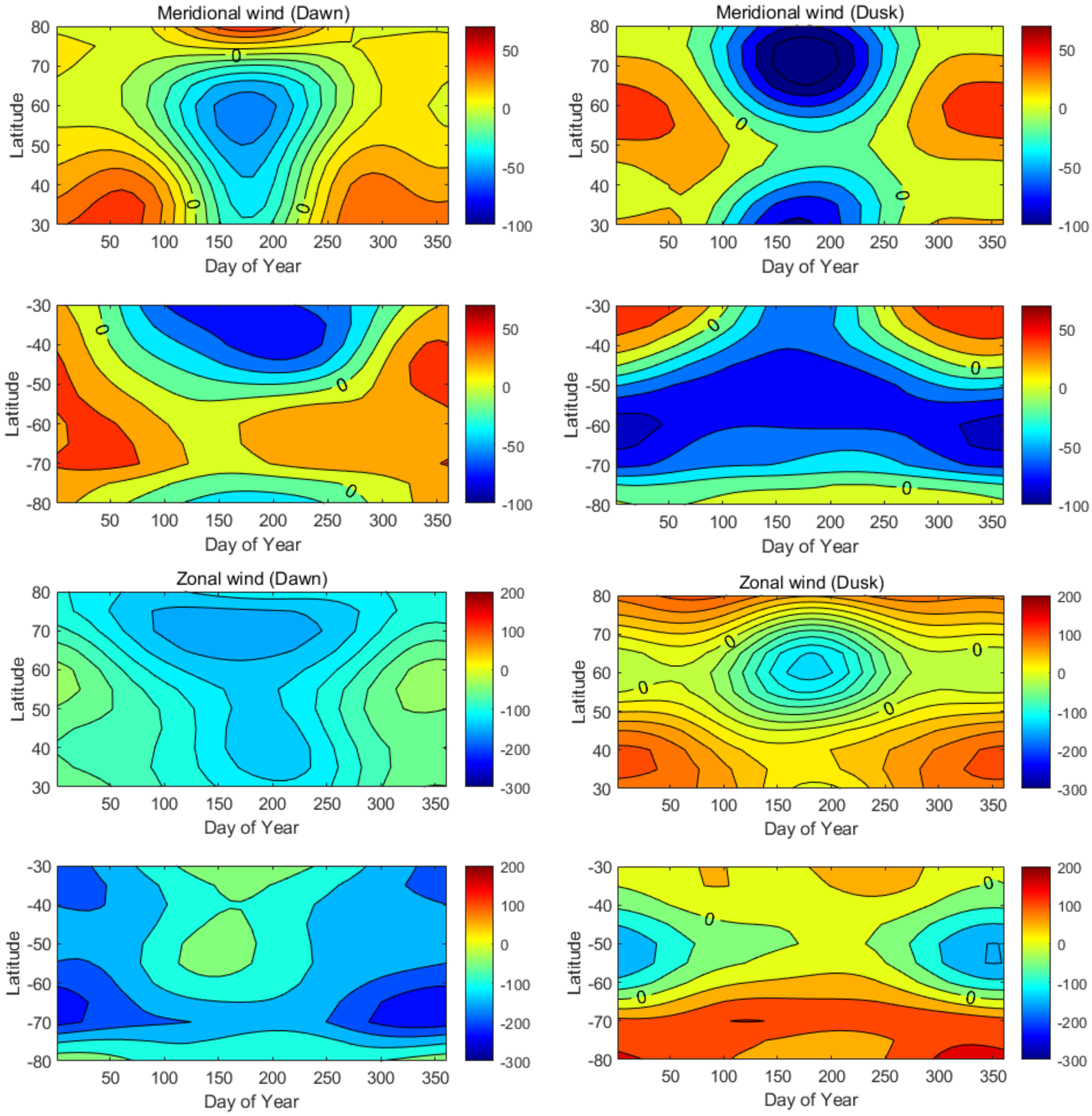

Figure 4. The latitudinal and seasonal variations of meridional (upper) and zonal (lower) wind at altitudes between 210 and 320 km at 0730LT (**left**) and 1930LT (**right**) from the HL-TWiM model.

Figure 5 shows the seasonal variation of $\Delta\rho_{rmax}$ and $\Delta\rho_{rmin}$ from APOD at dawn and dusk. The left panel shows that the annual maximum of $\Delta\rho_{rmax}$ from APOD occurs in July at both dawn and dusk. Xu et al. [10] showed that the annual maximum of $\Delta\rho_{rmax}$ from the GRACE observations occurred during equinoxes. The difference in peak occurrence time may be due to the different solar activity levels and local times. The results in Xu et al. [10] are averaged over all local times at high, middle, and low solar activity levels. The results from APOD in the paper are only for around the terminator at a low solar activity level. Xu et al. [30] and Shreedevit et al. [31] showed that the seasonal variation of ionospheric density at the high latitudes in the Southern Hemisphere has significant solar activity and local time dependence. Their results showed that the ionospheric density at the high latitudes of the Southern Hemisphere usually has a semiannual anomaly with peaks during the equinoxes for high and middle solar activity conditions, especially during the daytime. The larger ionospheric density may produce larger conductivity and Joule heating during the equinoxes. This could cause GRACE's largest longitudinal variations of thermospheric density to occur during the equinoxes. It has been reported that the ionospheric density at the high latitudes in the Southern Hemisphere has no significant semiannual anomaly and has a relatively low value during the equinoxes under low solar activity conditions (e.g., [30,31]). Thus, the $\Delta\rho_{rmax}$ from APOD in this paper has no significant peaks during the equinoxes.

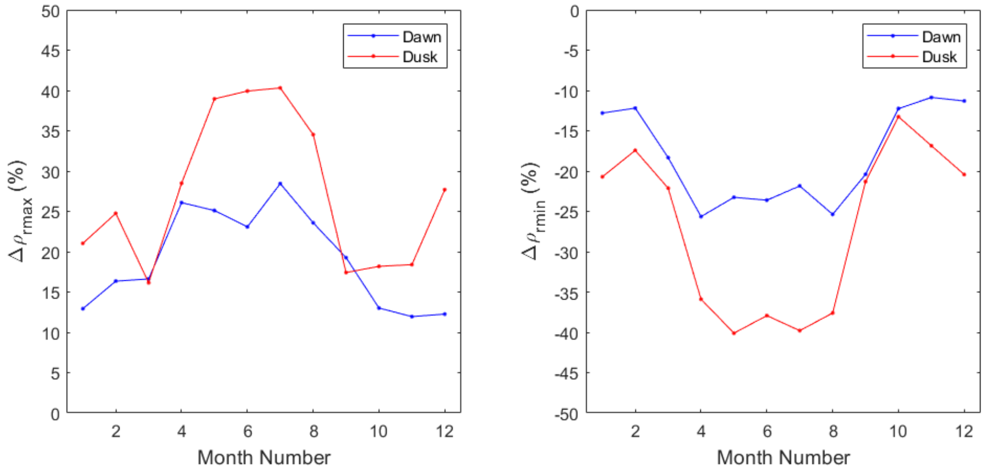

Figure 5. Seasonal variation of $\Delta\rho_{rmax}$ (**left**) and $\Delta\rho_{rmin}$ (**right**) at dawn and dusk from APOD. The blue and red lines denote the dawn and dusk sectors.

The left panel in Figure 5 shows that the annual maximum of $\Delta\rho_{rmax}$ from APOD reach 26.3% and 39.6% at dawn and dusk, respectively, in July, much greater than the annual maximum of $\Delta\rho_{rmax}$ at 480 km from GRACE value 15.2% [10]. The results from the GRACE observation in Xu et al. [10] are for all local times. According to the above results at dawn and dusk from APOD (see Figures 2 and 3), there are significant differences in the peak locations for different local times. So, the maxima of averaged $\Delta\rho_r$ for the two local times could be less than $\Delta\rho_{rmax}$ at dawn or dusk. Suppose all the observations at both dawn and dusk from APOD are used together to obtain the mean relative longitude variation around the terminator. In that case, the maximum will be ~24%, which is closer to the maximum from the GRACE data. So, the various locations of $\Delta\rho_{rmax}$ at different local times could bring the lower values of $\Delta\rho_{rmax}$ averaged for all local times. Furthermore, the data observed from 2017 to 2018 in 5° latitude × 1 month bins are used in this work, while the data from 2003 to 2008 in 10° latitude × 2 month bins were used by Xu et al. [10]. The different time windows and bins can also contribute to the different results. In addition, the difference in $\Delta\rho_{rmax}$ may also be due to the different solar activity levels in different years.

The left panel in Figure 5 shows that $\Delta\rho_{rmax}$ from APOD at dusk is significantly greater than at dawn in most months. For example, $\Delta\rho_{rmax}$ in June reaches 23.0% and 38.7% at dawn and at dusk, respectively. The difference in $\Delta\rho_{rmax}$ between dawn and dusk may be related to their different latitudes. From above, we know that $\Delta\rho_{rmax}$ is located at a higher latitude at dusk than at dawn around the solstices. Since a degree in longitude at a higher latitude represents a shorter length, the area of a higher-density region should be larger at dawn than at dusk. The larger area of the higher-density region should contribute to the lower $\Delta\rho_{rmax}$ at dawn. The observations from CHAMP [32] also show that the high-latitude density response is less significant around the dawn sector in both hemispheres.

The right panel in Figure 5 shows that $\Delta\rho_{rmin}$ from April to August is larger than in the other months. The annual minima of $\Delta\rho_{rmin}$ from APOD reach −25.6% and −40.1% at dawn and dusk. $\Delta\rho_{rmin}$ from APOD at dusk is significantly less than at dawn in most months. For example, $\Delta\rho_{rmax}$ in June reaches −23.6% and −37.9% at dawn and at dusk, respectively.

Figures 6 and 7 show the longitude variations of thermospheric density ($\Delta\rho_r$) from the MSIS 2.0 model at 460 km at dawn and dusk, respectively. Similar to the APOD data, the MSIS 2.0 predictions exhibit one zonal peak near the geomagnetic pole in the Northern and Southern Hemispheres. The annual maxima of $\Delta\rho_{rmax}$ in the Southern Hemisphere at dawn and dusk from MSIS 2.0 appear in August with values of 28.8% and 34.7%, respectively. The annual maximum of $\Delta\rho_{rmax}$ in the Northern Hemisphere from MSIS 2.0 occurs between December and February at dawn and dusk, and both values are ~14%. They are slightly less than the annual maxima from APOD. Figures 6 and 7 show that $\Delta\rho_{rmax}$ from MSIS 2.0 in the Southern Hemisphere is larger than those in the Northern Hemisphere at dawn and dusk from March to September. The MSIS annual maximum of $\Delta\rho_{rmax}$ appears in the Southern Hemisphere, as the results from APOD show. There are some differences between $\Delta\rho_{rmax}$ from APOD and MSIS 2.0. From November to February, $\Delta\rho_{rmax}$ from MSIS 2.0 in the Southern Hemisphere is larger, while $\Delta\rho_{rmax}$ from APOD in the Northern Hemisphere is larger. Take December as an example. In December, $\Delta\rho_{rmax}$ in the Northern Hemisphere from APOD is 13.2% and 25.4% at dawn and dusk, respectively. $\Delta\rho_{rmax}$ from MSIS 2.0 is only 9.0% and 14.3%, respectively. In the Southern Hemisphere, $\Delta\rho_{rmax}$ from APOD in December is only 9.0% and 7.1% at dawn and dusk, respectively. $\Delta\rho_{rmax}$ from the MSIS 2.0 model is 13.4% and 18.8%, respectively. Thus, $\Delta\rho_{rmax}$ from MSIS 2.0 appears in the Southern Hemisphere in all months. Correspondingly, $\Delta\rho_{rmax}$ from APOD appears in the Southern Hemisphere near the equinoxes and in the winter hemisphere around the solstices. The MSIS 2.0 model might overestimate the longitudinal variations of thermospheric density in the Southern Hemisphere and underestimate them in the Northern Hemisphere around the December solstice.

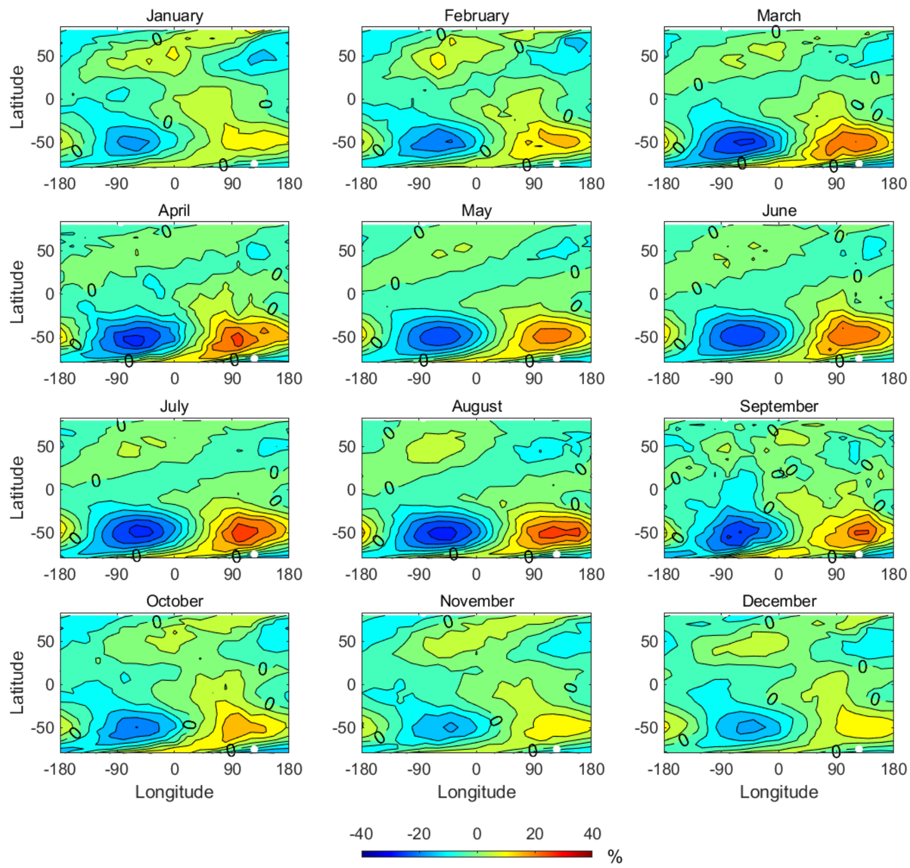

Figure 6. Same as Figure 2, except for the MSIS 2.0 model predictions.

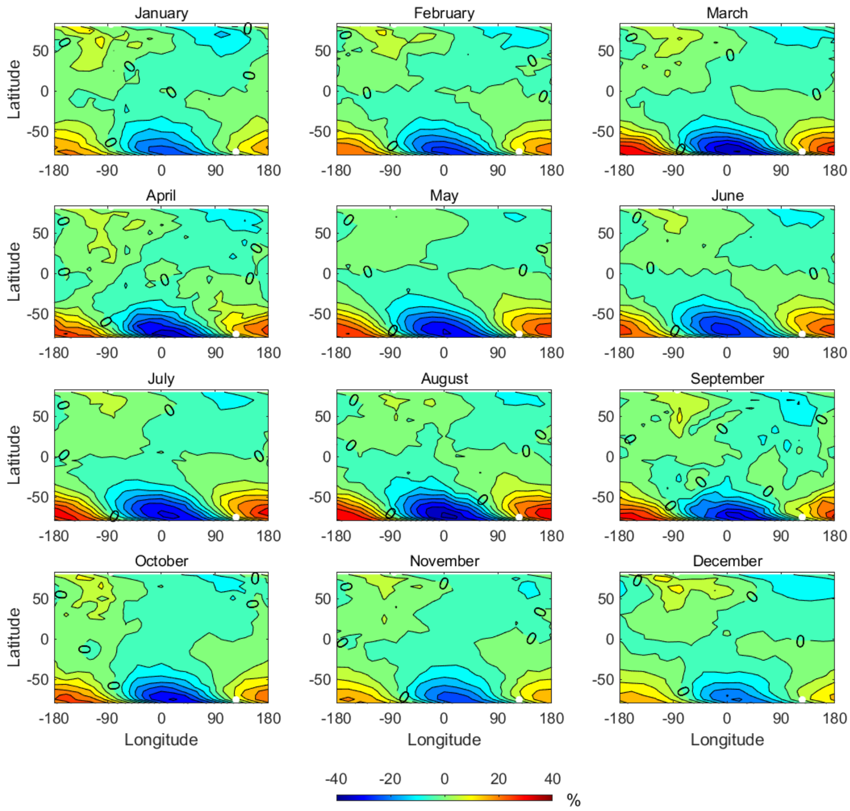

Figure 7. Same as Figure 3, except for the MSIS 2.0 model predictions.

As described above, the comparison of the APOD density between dusk and dawn indicates that $\Delta\rho_{rmax}$ at dusk from APOD is located at a higher latitude with larger values than at dawn. It can be seen in Figures 6 and 7 that the MSIS 2.0 results have the same characteristics. $\Delta\rho_{rmax}$ from MSIS 2.0 is located at 45–50° S and 45–60° N at dawn and located at 70–75° S and 60–75° N at dusk. It is the same as the observations in two hemispheres from APOD that $\Delta\rho_{rmax}$ from MSIS at dusk is located at a higher latitude than at dawn. In addition, it can be seen that the value of $\Delta\rho_{rmax}$ from MSIS 2.0 is also more pronounced at dusk than at dawn, similar to the result from APOD. For example, $\Delta\rho_{rmax}$ from the MSIS 2.0 model in August is 28.8% and 34.7% at dawn and dusk, respectively.

The thermospheric mass density is the product of the average molecular weight and number density. The thermospheric composition and number density also have complicated spatial and temporal variations [33]. To further analyze the cause of the longitudinal distribution of the thermospheric density, the average molecular weight and number density of the atmosphere at 460 km from the MSIS model are calculated. The relative longitudinal distribution of the average molecular weight and number density versus the zonal mean values at dawn and dusk are given, as shown in Figures 8–11, respectively. Figures 8–11 demonstrate both the atmospheric average molecular weight and number density maxima near the geomagnetic pole in the Northern or Southern Hemispheres. The maximum atmospheric average molecular weight appears in the winter hemisphere during the solstices, and the maximum atmospheric number density appears in the Southern Hemisphere. So $\Delta\rho_{rmax}$ from MSIS 2.0 is located in the winter hemisphere during the solstices, more pronounced in the Southern Hemisphere than in the Northern Hemisphere. In some sense, the longitudinal variation of $\Delta\rho_{rmax}$ from APOD should also be related to the distribution of the atmospheric average molecular weight from the MSIS model, as the average molecular weight from the model is used in the inversion of the atmospheric density [16]. More observational data are needed to verify the current study further.

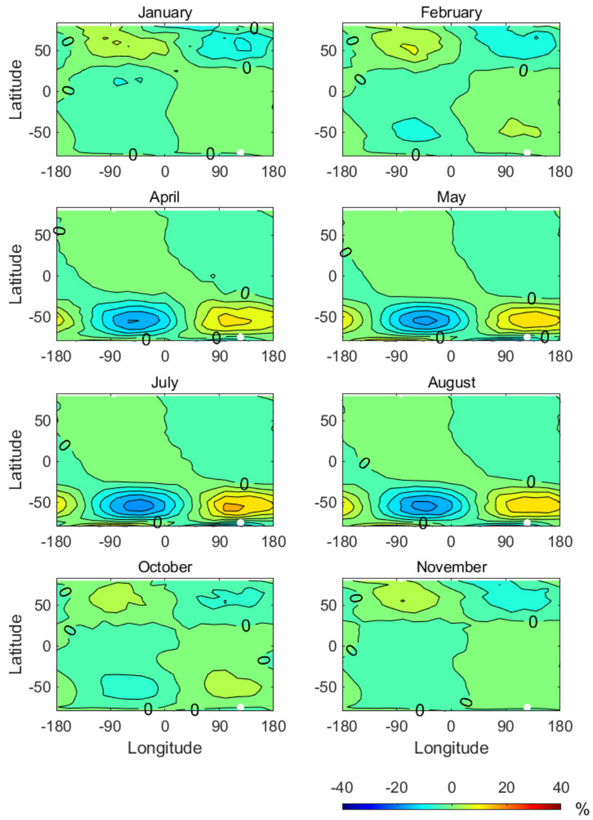

Figure 8. Same as Figure 6, except for the atmospheric average molecular weight.

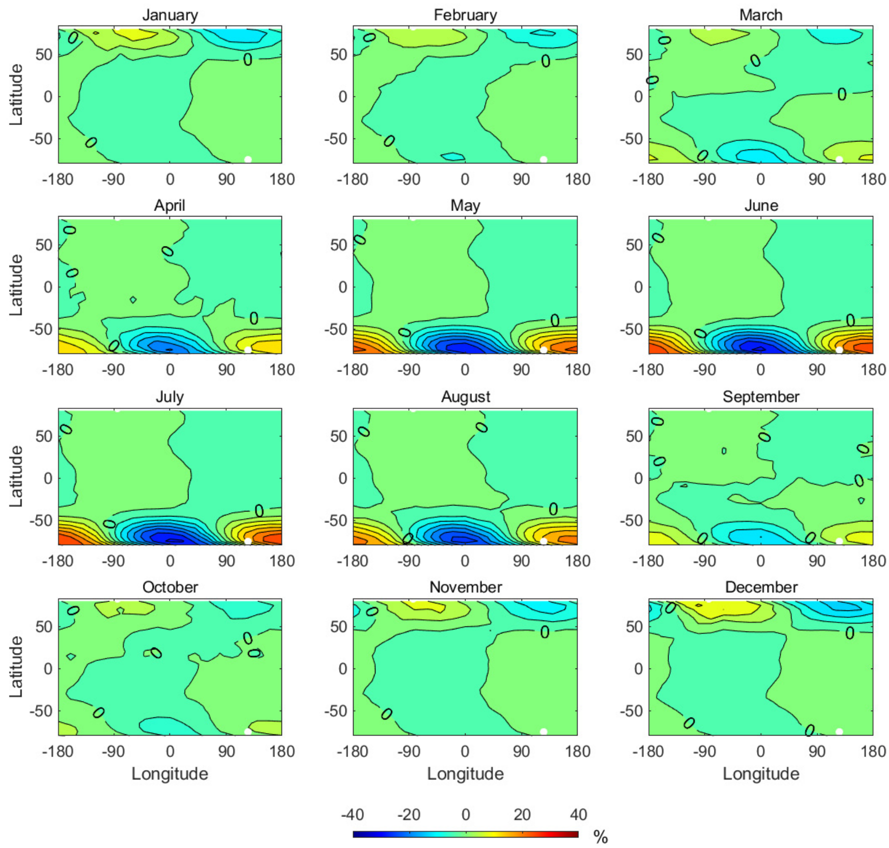

Figure 9. Same as Figure 7, except for the atmospheric average molecular weight.

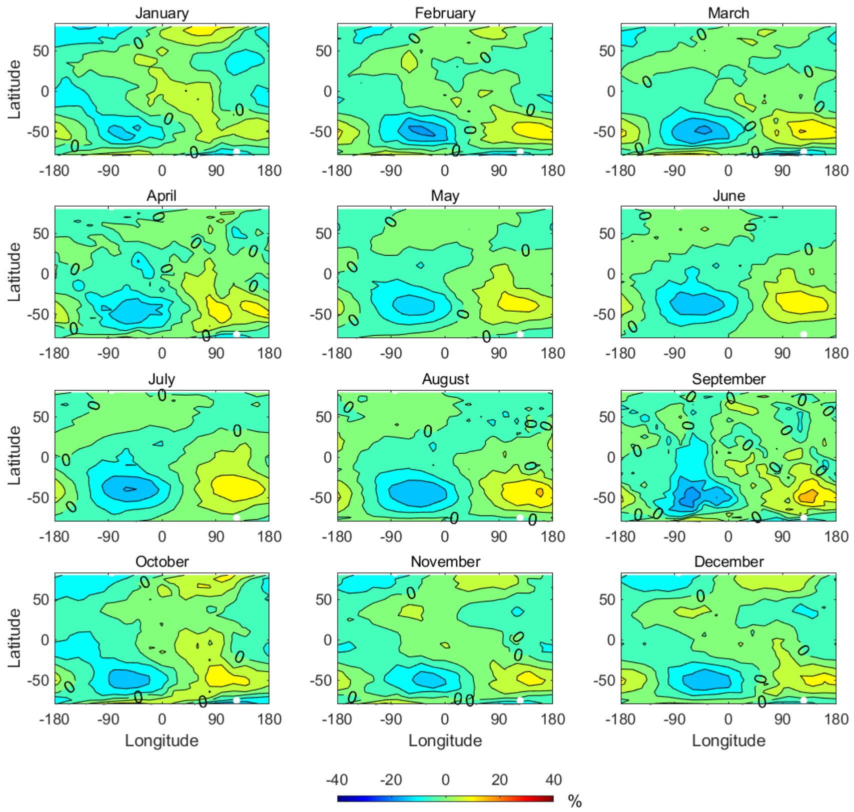

Figure 10. Same as Figure 6, except for the atmospheric number density.

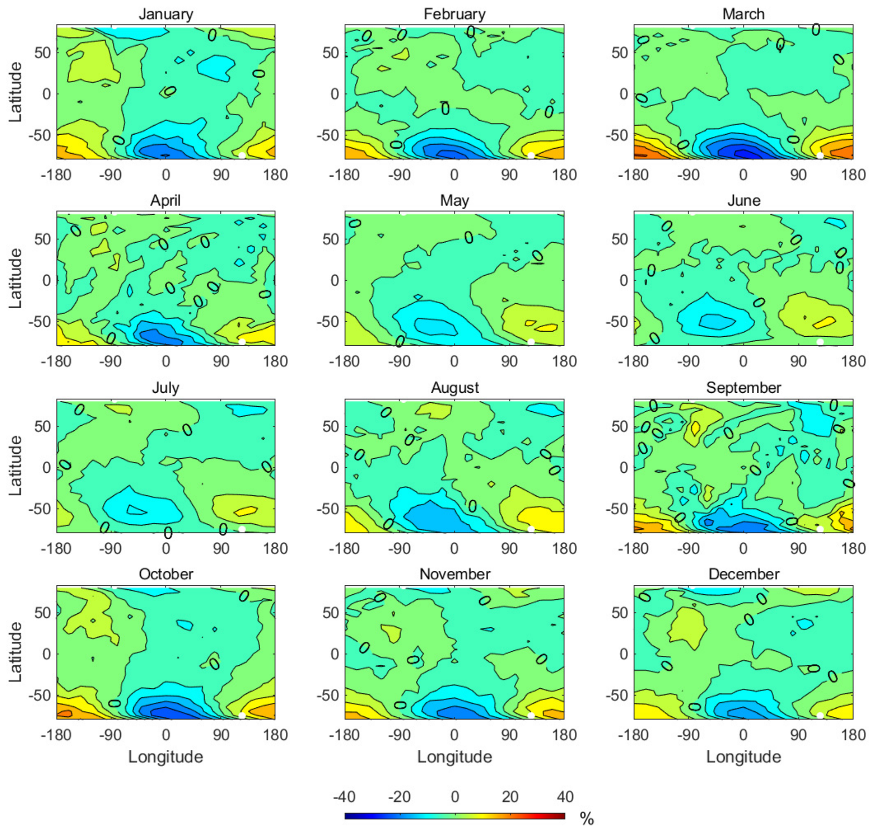

Figure 11. Same as Figure 7, except for the atmospheric number density.

Figures 12 and 13 show the longitudinal distribution of thermospheric temperature at 460 km from the MSIS model. There is a significantly high-temperature region around the geomagnetic pole at each hemisphere every month. The global maximum occurs in the southern hemisphere. The longitudinal distribution of the MSIS temperature is close to that of the MSIS density. The temperature denotes the thermal energy in the thermosphere. Thus, the longitudinal distribution of density could be related to the thermal energy and the atmospheric temperature. The high density and temperature region around the geomagnetic pole could be related to the aurora heating.

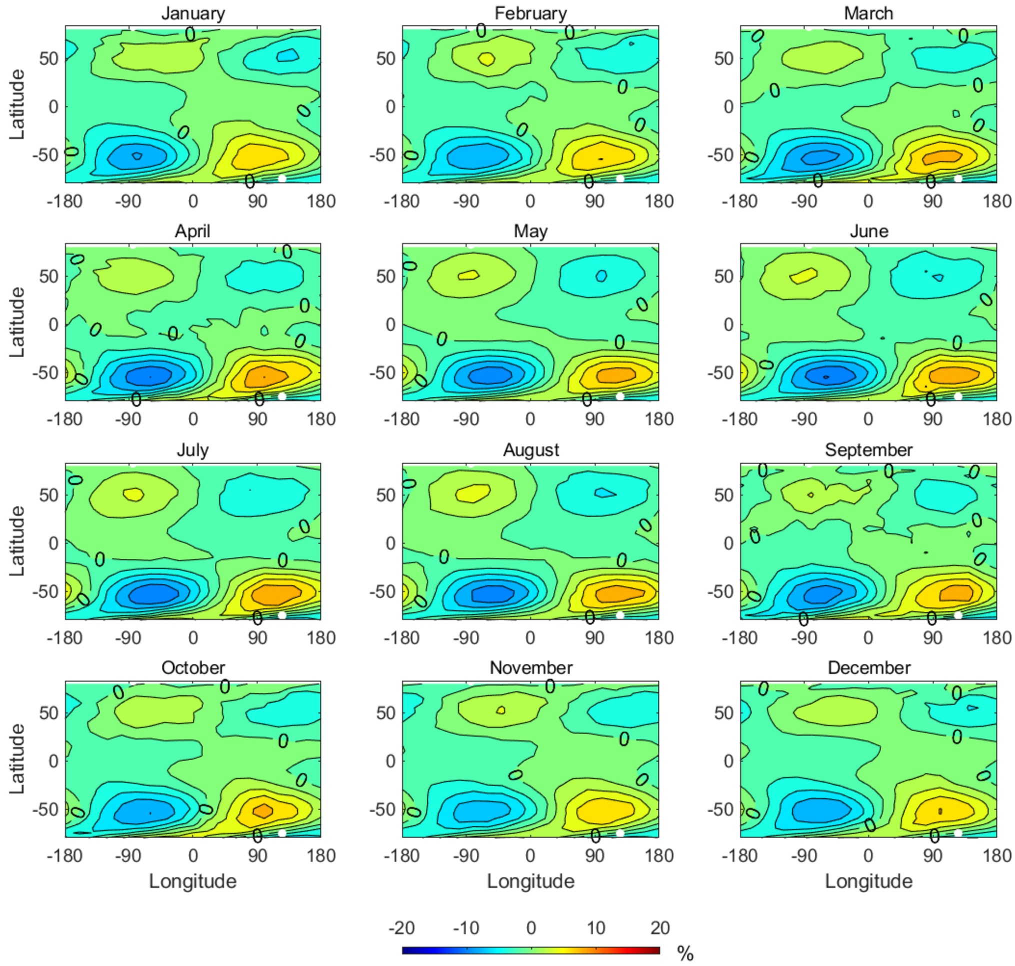

Figure 12. Same as Figure 6, except for the atmospheric temperature.

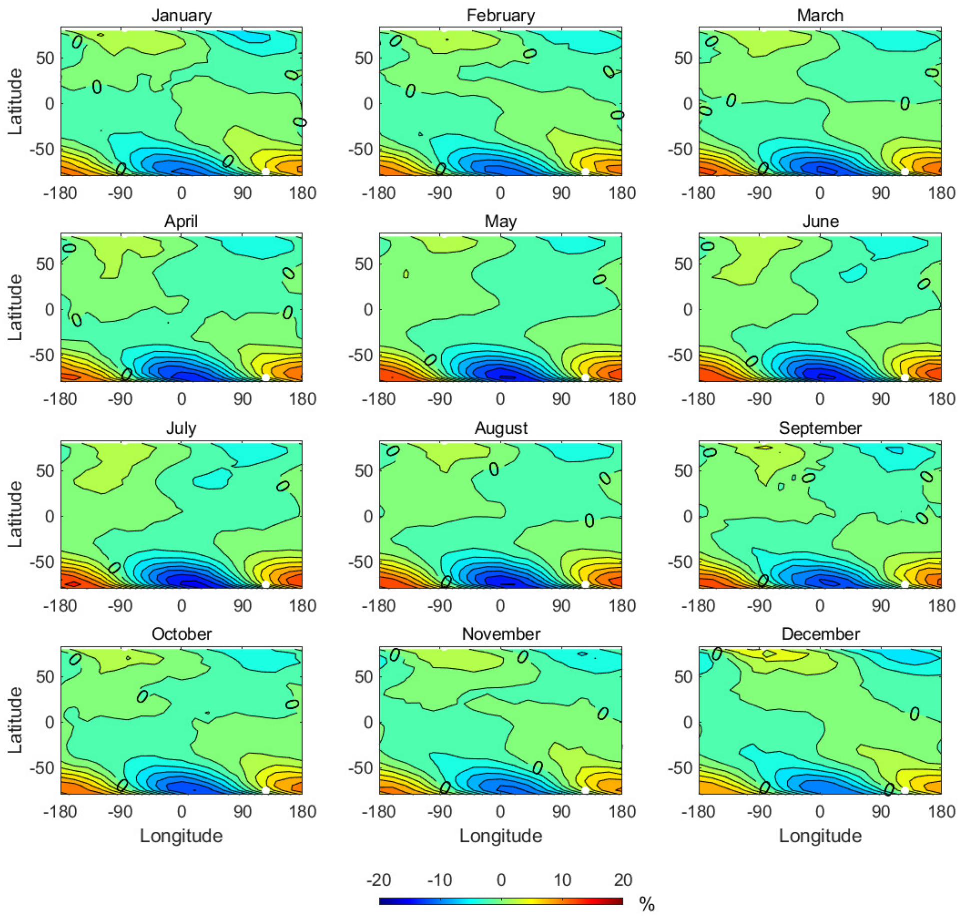

Figure 13. Same as Figure 7, except for the atmospheric temperature.

4. Conclusions

The paper focuses on the longitudinal distributions of upper thermospheric density at dawn and dusk under quiet geomagnetic conditions at low solar activity levels using the Atmospheric Density Detector (ADD) observations aboard the APOD satellite. The measurements from ADD/APOD are compared with the MSIS 2.0 model predictions. The relative longitudinal variations from the MSIS model density generally compare well with those from the observations. Both the APOD observations and the MSIS model predictions show a significant longitudinal variation of thermospheric density with maxima near the geomagnetic pole, especially in the winter hemisphere. The annual maxima of $\Delta\rho_{rmax}$ for APOD appear in the Southern Hemisphere around the July solstices. The values of maxima at dawn and dusk reach 26.3% and 39.6%, respectively. In most months of the year, $\Delta\rho_{rmax}$ at dusk for APOD is located at a higher latitude with larger values than at dawn. The auroral heating and meridional wind might play a significant role in the longitudinal variation of thermospheric density. The distribution of thermospheric density is related to the atmospheric average molecular weight from the MSIS model in some sense. More observational data are needed to verify the results of this study further.

Author Contributions: Conceptualization, G.C.; methodology, X.L.; software, X.L. and S.L.; validation, H.M.; formal analysis, G.C.; investigation, S.L.; resources, Y.L.; writing—original draft preparation, G.C.; writing—review and editing, M.H.; visualization, H.G. All authors have read and agreed to the published version of the manuscript.

Funding: This study was funded by the National Natural Science Foundation of China (41874183, 41474131 and 41604131) and the Pandeng Program of the National Space Science Center, Chinese Academy of Sciences. This research is also supported in part by the Youth Cross Team Scientific Research Project of the Chinese Academy of Sciences (JCTD-2021-10).

Institutional Review Board Statement: Not applicable.

Informed Consent Statement: Not applicable.

Data Availability Statement: The APOD data are provided by the Beijing Aerospace Control Center (ftp://36.110.27.60/product/APOD) (accessed on 10 October 2022). The NRLMSIS 2.0 code used in this work is available at https://map.nrl.navy.mil/map/pub/nrl/NRLMSIS/NRLMSIS2.0 (accessed on 10 January 2022). HL-TWiM Code used in this work is available at https://doi.org/10.5065/ad71-8827 (accessed on 28 May 2022). F10.7 and ap indexes are available at NASA OMNIWeb data explorer (http://celestrak.org/SpaceData/) (accessed on 28 November 2022).

Acknowledgments: The authors also gratefully acknowledge use of the MSIS 2.0 model and the HL-TWiM model.

Conflicts of Interest: The authors declare no conflict of interest. The funders had no role in the design of the study; in the collection, analyses, or interpretation of data; in the writing of the manuscript; or in the decision to publish the results.

References

1. Chen, G.-M.; Xu, J.; Wang, W.; Lei, J.; Burns, A.G. A comparison of the effects of CIR- and CME-induced geomagnetic activity on thermospheric densities and spacecraft orbits: Case studies. *J. Geophys. Res. Space Phys.* **2012**, *117*, A08315. [CrossRef]
2. Chen, G.-M.; Xu, J.; Wang, W.; Burns, A.G. A comparison of the effects of CIR- and CME-induced geomagnetic activity on thermospheric densities and spacecraft orbits: Statistical studies. *J. Geophys. Res. Space Phys.* **2014**, *119*, 7928–7939. [CrossRef]
3. Calabia, A.; Jin, S. Upper-Atmosphere Mass Density Variations from CASSIOPE Precise Orbits. *Space Weather* **2021**, *19*, e2020SW002645. [CrossRef]
4. Liu, H.; Lühr, H.; Henize, V.; Köhler, W. Global distribution of the thermospheric total mass density derived from CHAMP. *J. Geophys. Res. Earth Surf.* **2005**, *110*, A04301. [CrossRef]
5. Bhargawa, A.; Singh, A. Perceiving the Trend of Terrestrial Climate Change during the Past 40 Year (1978–2018). *J. Atmospheric Sci. Res.* **2021**, *4*, 2488. [CrossRef]
6. Singh, A.K.; Bhargawa, A. Ascendancy of Solar Variability on Terrestrial Climate: A review. *J. Basic Appl. Sci.* **2020**, *16*, 105–130.
7. Singh, A.; Bhargawa, A. Delineation of possible influence of solar variability and galactic cosmic rays on terrestrial climate parameters. *Adv. Space Res.* **2020**, *65*, 1831–1842. [CrossRef]
8. Bhargawa, A.; Singh, A.K. Solar irradiance, climatic indications and climate change-an empirical analysis. *Adv. Space Res.* **2019**, *64*, 271–277. [CrossRef]
9. Qian, L.; Solomon, S. Thermospheric Density: An Overview of Temporal and Spatial Variations. *Space Sci. Rev.* **2011**, *168*, 147–173. [CrossRef]
10. Xu, J.; Wang, W.; Gao, H. The longitudinal variation of the daily mean thermospheric mass density. *J. Geophys. Res. Space Phys.* **2013**, *118*, 515–523. [CrossRef]
11. Forbes, J.M.; Marcos, F.A.; Palo, S. Longitudinal structures in lower thermosphere density. *J. Geophys. Res. Earth Surf.* **1999**, *104*, 4373–4385. [CrossRef]
12. Forbes, J.M.; Zhang, X.; Bruinsma, S. Middle and upper thermosphere density structures due to nonmigrating tides. *J. Geophys. Res. Space Phys.* **2012**, *117*, A11306. [CrossRef]
13. Weng, L.; Lei, J.; Doornbos, E.; Fang, H.; Dou, X. Seasonal variations of thermospheric mass density at dawn/dusk from GOCE observations. *Ann. Geophys.* **2018**, *36*, 489–496. [CrossRef]
14. Liu, H.; Lühr, H.; Watanabe, S. A solar terminator wave in thermospheric wind and density simultaneously observed by CHAMP. *Geophys. Res. Lett.* **2009**, *36*, L10109. [CrossRef]
15. Li, X.; Xu, J.; Tang, G.; Chen, G.; Man, H.; Liu, S.; Li, Y. Processing and calibrating of in-situ atmospheric densities for APOD. *Chin. J. Geophys.* **2018**, *61*, 3567–3576. [CrossRef]
16. Tang, G.; Li, X.; Cao, J.; Liu, S.; Chen, G.; Man, H.; Zhang, X.; Shi, S.; Sun, J.; Li, Y.; et al. APOD mission status and preliminary results. *Sci. China Earth Sci.* **2019**, *63*, 257–266. [CrossRef]
17. Calabia, A.; Tang, G.; Jin, S. Assessment of new thermospheric mass density model using NRLMSISE-00 model, GRACE, Swarm-C, and APOD observations. *J. Atmos. Solar-Terr. Phys.* **2020**, *199*, 105207. [CrossRef]
18. Zhang, X.; Wang, Y.; Cai, Q.; Chen, G. Seasonal Oscillations of Thermosphere Neutral Density at Dusk/Dawn as Measured by Three Satellite Missions. *J. Geophys. Res. Space Phys.* **2022**, *127*, e2021JA030197. [CrossRef]
19. Emmert, J.T.; Drob, D.P.; Picone, J.M.; Siskind, D.E.; Jones Jr, M.; Mlynczak, M.G.; Yuan, T. NRLMSIS 2.0: A whole-atmosphere empirical model of temperature and neutral species densities. *Earth Space Sci.* **2021**, *8*, e2020EA001321.
20. Picone, J.M.; Hedin, A.E.; Drob, D.P.; Aikin, A.C. NRLMSISE-00 empirical model of the atmosphere: Statistical comparisons and scientific issues. *J. Geophys. Res.* **2002**, *107*, 1468. [CrossRef]
21. Ma, R.; Xu, J.; Wang, W.; Lei, J.; Liu, H.-L.; Maute, A.; Hagan, M.E. Variations of the nighttime thermospheric mass density at low and middle latitudes. *J. Geophys. Res. Earth Surf.* **2010**, *115*, A12301. [CrossRef]

22. Emmert, J.; Warren, H.; Segerman, A.; Byers, J.; Picone, J. Propagation of atmospheric density errors to satellite orbits. *Adv. Space Res.* **2017**, *59*, 147–165. [CrossRef]
23. Dhadly, M.S.; Emmert, J.T.; Drob, D.P.; Conde, M.G.; Aruliah, A.; Doornbos, E.; Shepherd, G.G.; Wu, Q.; Makela, J.J.; Niciejewski, R.J.; et al. HL-TWiM Empirical Model of High-Latitude Upper Thermospheric Winds. *J. Geophys. Res. Space Phys.* **2019**, *124*, 10592–10618. [CrossRef]
24. Shepherd, S.G. Altitude-adjusted corrected geomagnetic coordinates: Definition and functional approximations. *J. Geophys. Res. Space Phys.* **2014**, *119*, 7501–7521. [CrossRef]
25. Pulkkinen, T.I.; Tanskanen, E.I.; Viljanen, A.; Partamies, N.; Kauristie, K. Auroral electrojets during deep solar minimum at the end of solar cycle 23. *J. Geophys. Res. Atmos.* **2011**, *116*, A04207. [CrossRef]
26. Gao, H.; Xu, J.; Chen, G.; Zhu, Y.; Liu, W.; Wang, C. Statistical Structure of Nighttime O_2 Aurora from SABER and Its Dependence on Geomagnetic and Solar Activities in Winter. *J. Geophys. Res. Space Phys.* **2020**, *125*, e2020JA028302. [CrossRef]
27. Yu, C.; Zhang, X.; Wang, W.; He, F. Longitudinal Dependence of Ionospheric Poynting Flux in the Northern Hemisphere During Quite Times. *J. Geophys. Res. Space Phys.* **2021**, *126*, e2021JA029717. [CrossRef]
28. Wang, X.; Miao, J.; Lu, X.; Aa, E.; Liu, J.; Wang, Y.; Liu, S. Latitudinal Impacts of Joule Heating on the High-Latitude Thermospheric Density Enhancement During Geomagnetic Storms. *J. Geophys. Res. Space Phys.* **2021**, *126*, e2020JA028747. [CrossRef]
29. Xu, J.; Smith, A.K.; Wang, W.; Jiang, G.; Yuan, W.; Gao, H.; Yue, J.; Funke, B.; López-Puertas, M.; Russell, J.M. An observational and theoretical study of the longitudinal variation in neutral temperature induced by aurora heating in the lower thermosphere. *J. Geophys. Res. Space Phys.* **2013**, *118*, 7410–7425. [CrossRef]
30. Xu, S.; Zhang, B.-C.; Liu, R.-Y.; Guo, L.-X.; Wu, Y.-W. Comparative studies on ionospheric climatological features of NmF2 among the Arctic and Antarctic stations. *J. Atmos. Solar-Terr. Phys.* **2014**, *119*, 63–70. [CrossRef]
31. Shreedevi, P.; Choudhary, R.; Yu, Y.; Thomas, E.G. Morphological study on the ionospheric variability at Bharati, a polar cusp station in the southern hemisphere. *J. Atmos. Solar-Terr. Phys.* **2019**, *193*, 105058. [CrossRef]
32. Yamazaki, Y.; Kosch, M.J.; Sutton, E.K. North-south asymmetry of the high-latitude thermospheric density: IMF B_Y effect. *Geophys. Res. Lett.* **2015**, *42*, 225–232. [CrossRef]
33. Qian, L.; Gan, Q.; Wang, W.; Cai, X.; Eastes, R.; Yue, J. Seasonal Variation of Thermospheric Composition Observed by NASA GOLD. *J. Geophys. Res. Space Phys.* **2022**, *127*, e2022JA030496. [CrossRef] [PubMed]

Disclaimer/Publisher's Note: The statements, opinions and data contained in all publications are solely those of the individual author(s) and contributor(s) and not of MDPI and/or the editor(s). MDPI and/or the editor(s) disclaim responsibility for any injury to people or property resulting from any ideas, methods, instructions or products referred to in the content.